



## DWT-DCT Image Watermarking with Quantum-inspired Optimization

Nova Rijati<sup>1</sup>      Sudipta Kr. Ghosal<sup>2</sup>      Aditya Kumar Sahu<sup>3</sup>      Aceng Sambas<sup>4,5,6</sup>  
 De Rosal Ignatius Moses Setiadi<sup>1,7,\*</sup>

<sup>1</sup>Faculty of Computer Science, Universitas Dian Nuswantoro, Semarang, Central Java 50131, Indonesia

<sup>2</sup>Department of Cyber Forensics and Information Security, Behala Government

Polytechnic, 756, Upendra Nath Banerjee Road, Parnasree, Behala, Kolkata-700060, India

<sup>3</sup>Amrita School of Computing, Amrita Vishwa Vidyapeetham, Amaravati, Andhra Pradesh 522503, India

<sup>4</sup>Faculty of Informatics and Computing,

Universiti Sultan Zainal Abidin, Campus Besut, 22200 Terengganu, Malaysia

<sup>5</sup>Artificial Intelligence for Sustainability and Islamic Research Center (AISIR),

Universiti Sultan Zainal Abidin, Gongbadak 21300, Malaysia

<sup>6</sup>Department of Mechanical Engineering,

Universitas Muhammadiyah Tasikmalaya, Tamansari Gobras 46196 Tasikmalaya, Indonesia

<sup>7</sup>Research Center for Quantum Computing and Materials Informatics, Faculty of Computer Science,

Universitas Dian Nuswantoro, Semarang 50131, Indonesia

\* Corresponding author's Email: [moses@dsn.dinus.ac.id](mailto:moses@dsn.dinus.ac.id)

---

**Abstract:** This study presents a robust and imperceptible image watermarking method combining Discrete Wavelet Transform (DWT), Discrete Cosine Transform (DCT), and quantum-inspired optimization. The approach applies DWT to decompose the image into subbands and embeds the watermark in the low-frequency subband. DCT is used to identify Alternating Current (AC) coefficients, with Quantum-Inspired Annealing (QIA) optimizing their selection and Quantum Variational Circuits (QVC) dynamically adjusting the embedding intensity ( $\alpha$ ) for each block. The novelty of this study lies in integrating QIA and QVC to optimize both the embedding position and intensity, enabling a more adaptive and robust watermarking mechanism compared to existing quantum-inspired methods. Experimental results in standard images show high imperceptibility, with average Peak signal-to-noise ratio (PSNR) and Structural Similarity Index Measurement (SSIM) values of 46.93 dB and 0.9979, respectively. The method demonstrates strong robustness, achieving an average Normalized Correlation (NC) of 0.9752 across various attacks, including JPEG compression, noise addition, and cropping. Compared to existing methods, the proposed approach performs better in maintaining watermark quality and robustness. This study highlights the potential of quantum-inspired techniques in watermarking, offering a promising direction for further research and real-world applications.

**Keywords:** Quantum-classic watermarking, Quantum image watermarking, Quantum-inspired optimization, Quantum optimization, Quantum variational circuits.

---

### 1. Introduction

Digital watermarking has become a significant technique in protecting copyright and ensuring the integrity of digital content, especially in the digital era full of challenges in data security. In robust watermarking, it is important to ensure that the watermark remains protected and is not easily damaged, even though it is subjected to various

attacks [1]. The use of domain transformation has been widely applied in watermarking to improve the resilience of watermarks because this domain allows watermarks to be inserted at more stable and protected frequencies [1, 2].

Domain transformation methods such as Discrete Wavelet Transform (DWT) and Discrete Cosine Transform (DCT) are often used to improve the resilience of watermarking because both have

characteristics that support the success of robust and imperceptible watermarks [3]. In addition, DWT and DCT are often used in image compression, allowing watermarks to remain robust even after JPEG or JPEG 2000 compression is applied. DWT divides the image into four main frequency subbands at each transformation level: LL (Low-Low), LH (Low-High), HL (High-Low), and HH (High-High) [4]. The LL subband, which contains the most significant information of the image, is more stable and resistant to external disturbances, making it an ideal location for watermark embedding [5]. On the other hand, high-frequency subbands such as LH, HL, and HH contain image details susceptible to changes due to noise or compression. The selection of the LL subband allows the watermark to resist manipulation while maintaining the image's visual quality. In addition, DWT enables multi-resolution analysis, which is useful for balancing watermark robustness and imperceptibility.

Meanwhile, DCT converts the spatial signal into the frequency domain, where the image energy is compressed on the main coefficients, making it more efficient in representing the image [6–8]. DCT produces two kinds of coefficients, namely one Direct Current (DC) coefficient and the rest are many Alternating Current (AC) coefficients [9]. The DC coefficient represents the average intensity of the block and greatly affects the overall appearance [10]. Watermark embedding on the DC coefficient is generally very strong but can reduce the imperceptibility of the image. In contrast, the AC coefficients, which represent the mid- and high-frequency components, are more suitable for watermark Embedding because they impact the visual quality less. Some AC coefficients are also resistant to lossy compression, making them a better choice for maintaining watermark robustness after compression, such as when applying JPEG [11]. By choosing the right position of AC coefficients, watermarks can be embedded efficiently, maintaining a balance between the imperceptibility and robustness of the watermark.

The combination of DWT and DCT provides a more robust approach to watermarking. DWT separates the image into subbands, with the more stable LL subband selected as the watermark embedding location [9]. The DCT transform is then applied to the LL subband, and the watermark is embedded at the AC coefficients. The selection of AC coefficients in the LL subband is crucial because it can affect both the watermark robustness and the visual quality. If the position of the AC coefficients is not selected correctly, the robustness of the watermark can be reduced. Therefore, selecting the

optimal position of the AC coefficients is very important to balance the imperceptibility and robustness of the watermark.

Applying optimization methods to the embedding process offers great potential to improve the security of watermarks. Several methods have been applied to optimize messages or watermarks in data hiding methods, for example, using genetic algorithms [12, 13], Artificial Bee Colony [14], Gradient-based Optimizer [15], Grey Wolf Optimizer [16], etc. Inspired by quantum annealing[17], the Quantum-Inspired Annealing (QIA) method can be applied to determine the optimal AC position for Embedding. This technique allows for increased watermark robustness without sacrificing excessive image quality, providing an efficient solution for adjusting the embedding position in the DCT block. In addition, inspired by quantum computing, pure quantum computing has also begun to be widely applied in watermarking[18].

Quantum Variational Circuits (QVC) [19] is a quantum method that can optimize the embedding intensity or alpha parameter. QVC functions to adjust the appropriate watermark intensity in each DCT block, ensuring that the watermark is invisible but still has high resistance to removal or modification attempts. This approach allows for more efficient alpha dynamic adjustment, increasing the complexity for unauthorized parties trying to remove the watermark without being detected [4].

The evaluation of watermarking performance in this study includes image quality, robustness, and imperceptibility of the watermark. With quantum-based optimization, this method is expected to increase the watermark's resilience to various attacks, such as compression and manipulation. The main contributions of this study are as follows:

1. Integrating Quantum-Inspired Annealing to determine the optimal position of AC coefficients in the DCT domain.
2. Applying Quantum Variational Circuits (QVC) to adjust the alpha value adaptively to enable optimal embedding intensity for each block.
3. Producing a watermarking method based on a combination of DWT-DCT transformations that is robust and has optimal imperceptibility.

The rest of this paper is structured as follows. Section 2 reviews the related literature, providing insights into current watermarking techniques and their limitations. Section 3 introduces the proposed DWT-DCT watermarking method with quantum-based optimization, including a detailed description of the QIA and QVC approaches. Section 4 presents the experimental results and analysis, focusing on evaluating image quality using PSNR and SSIM and

robustness against various manipulative attacks with NC. Finally, Section 5 concludes the research findings and outlines future development directions.

## 2. Related works

In recent years, various studies have been conducted to improve the robustness and imperceptibility of digital watermarking. The main challenge in watermarking lies in optimizing the parameters and positions of the Embedding to achieve an ideal balance between robustness and imperceptibility. Transform-based watermarking methods such as DCT and DWT dominate the research due to their resistance to signal processing attacks [9]. Various studies have explored metaheuristic optimization algorithms to improve the embedding quality. For example, Gao and Chen [14] proposed a hybrid approach combining DWT-SVD with an improved Artificial Bee Colony algorithm to optimize the scale factor dynamically. This approach shows superior performance in terms of imperceptibility and robustness by balancing both attributes through effective optimization.

Melman and Evsutin [15] developed a Gradient-Based Optimizer (GBO)-based method to regularize the DCT coefficients, ensuring that the watermark embedding maintains high imperceptibility and robustness. Their objective function integrates PSNR and SSIM metrics, emphasizing the role of optimization in refining the DCT coefficients of block-based transforms. Hu et al. [16] used the Grey Wolf Optimizer (GWO) algorithm to adjust the DCT coefficients adaptively. This approach leverages entropy-based adjustment to improve the visual quality and robustness, especially in JPEG compression scenarios. In addition, visual enhancement techniques such as denoising autoencoders further enhance the watermark recovery quality.

Several studies have highlighted the importance of adaptivity in embedding strategies. Wang et al. [6] proposed a DCT-based watermarking method that varies the quantization steps across different image layers, resulting in high embedding capacity and robustness. This adaptive approach was also applied to color images, demonstrating the flexibility of frequency domain methods in various applications. Furthermore, hybrid schemes such as DWT-DCT optimization have shown promising results [20]. For example, Budiman et al. [12] optimized the block-based DWT coefficients using a genetic algorithm to fine-tune the trade-off between robustness and imperceptibility. This method demonstrates the

importance of combining different transformations and optimization algorithms.

Recently, quantum computing has gained attention due to its various advantages. Including watermarking technology, quantum computing has begun to be researched and applied. For example Xing et al. [21] introduced a geometrically invariant quantum watermarking scheme combining Quantum Error Correction (QEC) with Geometric Transformation-based Image Assembling (GTA). Their approach focuses on improving robustness against geometric attacks, including cropping and rotation, using Quantum Image Rotation (QIR) and Quantum Block Rotation (QBR). However, this method primarily emphasizes geometric robustness and lacks adaptive intensity adjustments for embedding coefficients.

Similarly, Yuan et al. [22] proposed a scheme utilizing the New Enhanced Quantum Image Representation (NEQR) and Quantum Majority Finder (QMF) to embed watermarks into carrier images uniformly. While their method demonstrates good visual quality and robustness, it relies on uniform embedding rules, limiting its adaptability to varying image features. Aly [23] extended quantum watermarking to color images using the New Quantum Binary Image Detector (NQPID) and quantum polar block representation. This technique enhances security and storage efficiency but primarily addresses color image domains and does not explore dynamic optimization of embedding parameters for grayscale or frequency-domain watermarking.

Although metaheuristic-based optimization methods have achieved significant progress, some challenges remain. Most optimization-based watermarking techniques rely on classical metaheuristic algorithms, which, although effective, are limited in their ability to adjust embedding parameters for each image block dynamically. This study addresses these limitations by introducing QIA and QVC [19] into the watermarking process. In contrast to Xing et al. [21], who focused on geometric robustness, while Yuan et al. [22] focus on uniform embedding and Aly [23] focus on spatial domain and color-specific applications, respectively, this study leverages QVC to adaptively adjust the embedding intensity ( $\alpha$ ) for each DCT block, achieving a more precise trade-off between imperceptibility and robustness. QIA exploits quantum-inspired search principles to enhance robustness, while QVC ensures optimal embedding intensity through quantum superposition and entanglement properties. Thus, this approach provides a solid foundation for further

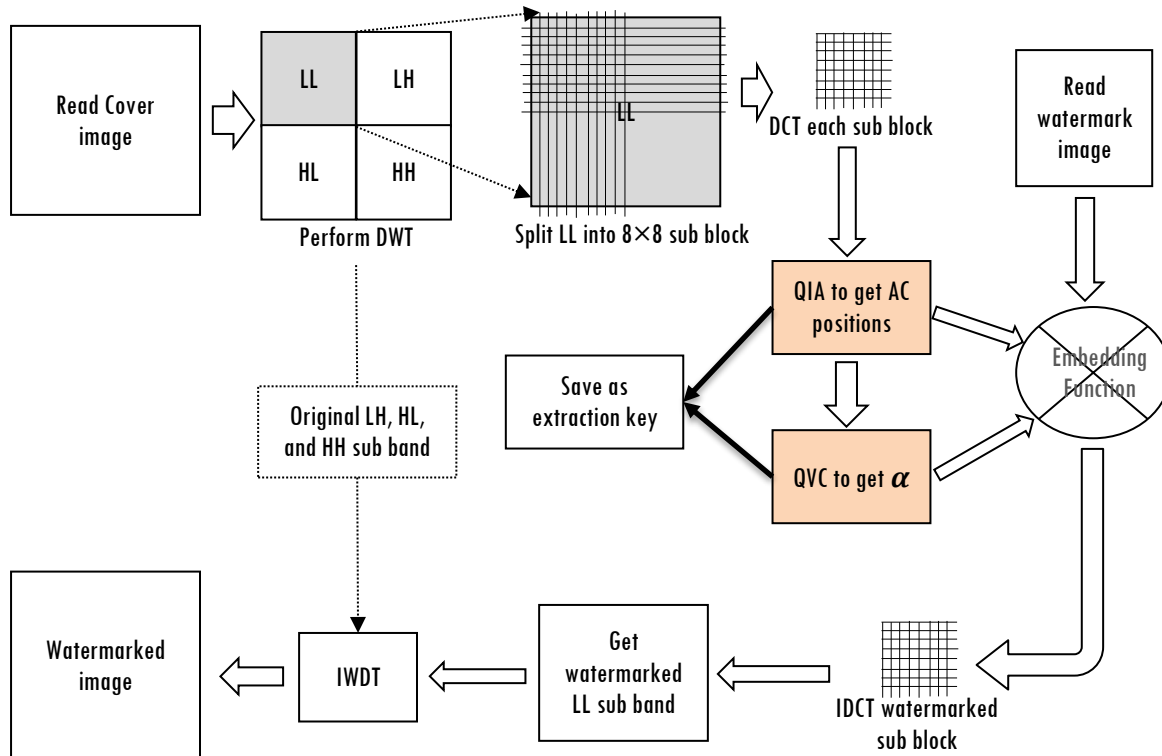


Figure. 1 Overview of Proposed method

exploration in applying quantum computing in image watermarking.

### 3. Proposed method

#### 3.1 Overview of proposed system

The proposed watermarking method combines DWT and DCT to enhance the robustness and imperceptibility of the watermark with quantum-based techniques for adaptive Embedding. The system flow consists of several stages: applying DWT to identify significant subbands, performing DCT on the LL subband, and embedding the watermark on the optimized AC coefficients using QIA and QVC. The schematic diagram of the system in Figure 1 illustrates the overall process.

#### 3.2 DWT-DCT transformation

This stage involves applying DWT to the cover image ( $I$ ) to decompose the image into four frequency subbands, namely LL, LH, HL, and HH. The DWT decomposition can be expressed in Eq. (1). Each subband represents a different spatial frequency, and the LL subband contains the most significant information and is the most resistant to attacks [24].

$$DWT(I) = \{LL, LH, HL, HH\} \tag{1}$$

After DWT decomposition, DCT is applied to each  $8 \times 8$  block within the LL subband to isolate the frequency components, thus providing an optimal domain for Embedding. DCT transforms the  $8 \times 8$  spatial block  $B$  into  $D$  frequencies, as in Eq (2).

$$D_{u,v} = \frac{1}{4} \sum_{x=0}^7 \sum_{y=0}^7 B_{x,y} \cos\left(\frac{(2x+1)u\pi}{16}\right) \cos\left(\frac{(2y+1)v\pi}{16}\right) \tag{2}$$

where  $u, v$  represent the frequency coordinates.

This transformation produces DC coefficients and AC coefficients representing low and high frequencies. To maintain visual quality and robustness, only selected AC coefficients are used for watermark embedding, while DC coefficients representing the average intensity of the block are left unchanged.

#### 3.3 Quantum-inspired annealing (QIA)

QIA is used to find the optimal AC coefficient position on each  $8 \times 8$  block in the LL subband of the DCT transformation. QIA is applied to minimize the loss function, which considers robustness and imperceptibility.

Given the DCT-transformed block  $D$ , a set of initial AC positions  $P = \{(u_1, v_1), (u_2, v_2)\}$  is

proposed, and the annealing process iteratively adjusts these positions to minimize the objective function using Eq (3).

$$L(P, \alpha) = \text{mean} \left( \left| \text{IDCT}(\text{embed}(D, P, \alpha)) - \text{IDCT}(D) \right|^2 \right) \quad (3)$$

Where  $\alpha$  is the embedding intensity optimized later, and IDCT denotes the Inverse Discrete Cosine Transform. This function balances embedding strength with minimal perceptual distortion. The final selected positions  $(u, v)$  are used for watermark embedding, optimizing both AC positions and coefficient values.

### 3.4. Adaptive embedding using quantum variational circuits (QVC)

QVC determines the adaptive embedding intensity  $\alpha$  in each  $8 \times 8$  block. QVC uses a series of quantum circuits with four qubits to dynamically generate the optimal  $\alpha$ . The circuit starts with Hadamard gates ( $H$ ) to create a superposition state, followed by parameterized  $RY$  rotations based on a set of parameters  $\theta = (\theta_1, \theta_2, \dots, \theta_n)$ , and  $CNOT$  for entanglement[25]–[27]. The structure of this circuit is represented by Equation (4). After executing the circuit, the expectation value  $\langle Z \rangle$  is measured on each qubit. As an illustration of the quantum circuit, see Fig. 2.

$$|\psi(\theta)\rangle = \prod_{i=1}^n H(q_i) \prod_{i=1}^n RY(\theta_i) \prod_{j=1}^{n-1} CNOT(q_j, q_{j+1}) |0\rangle \quad (4)$$

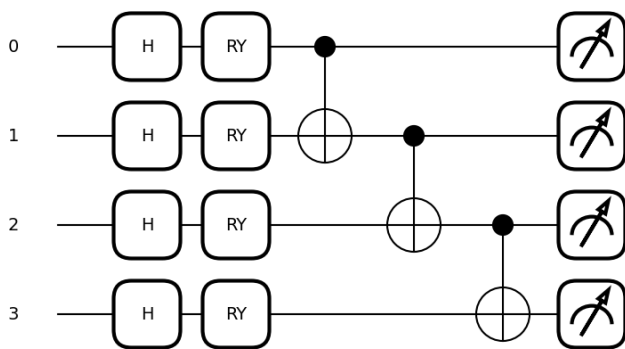


Figure. 2 QVC circuit design for calculating  $\alpha$  parameter

The final  $\alpha$  value is computed by taking the average expectation of the Pauli-Z values across all qubits, as shown in Equation (5). This averaged  $\alpha$  ensures that the embedding intensity is adapted based on the collective state of all qubits, which allows for a more robust and dynamically optimized embedding process.

$$\alpha = \frac{1}{n} \sum_{i=1}^n \langle Z_i \rangle \quad (5)$$

All QIA and QVC data are stored as extraction keys, so these two processes are used only in the embedding process.

### 3.5 Embedding and extraction process

#### 3.5.1 Embedding

The embedding process is carried out after performing the DWT-DCT transformation that has been explained previously, as well as the QIA and QVC processes for optimization. Specifically, we use a binary image as a watermark (watermark pixels  $w$  have values 0 and 1). The embedding process is carried out on the selected AC coefficient  $(u, v)$  and with the specified  $\alpha$  value. The Embedding is done with Eq. (6).

$$\begin{cases} w = 1, D[u_1, v_1] = \min(D[u_1, v_1], D[u_2, v_2]) \cdot \alpha \\ \text{and } D[u_2, v_2] = \max(D[u_1, v_1], D[u_2, v_2]) \cdot \alpha \\ w = 0, D[u_1, v_1] = \max(D[u_1, v_1], D[u_2, v_2]) \cdot \alpha \\ \text{and } D[u_2, v_2] = \min(D[u_1, v_1], D[u_2, v_2]) \cdot \alpha \end{cases} \quad (6)$$

After embedding all bits, the IDCT and inverse DWT are applied to reconstruct the watermarked image. Eq. (7) is performed for IDCT on each  $8 \times 8$  block. After all blocks in the LL subband are reconstructed using IDCT, IDWT is applied to restore the watermarked image to the original spatial domain. IDWT recombines the LL, LH, HL, and HH subbands generated from the initial DWT. IDWT can be expressed by Eq. (8) for a given LL subband embedding and other subbands.

$$B_{x,y} = \frac{1}{4} \sum_{u=0}^7 \sum_{v=0}^7 D_{u,v} \cos\left(\frac{(2x+1)u\pi}{16}\right) \cos\left(\frac{(2y+1)v\pi}{16}\right) \quad (7)$$

Where  $B_{x,y}$  is the pixel value at position  $(x, y)$  in the reconstructed spatial block.  $D_{u,v}$  is the DCT coefficient at frequencies  $x, y$  representing the pixel coordinates in the block, and  $u, v$  is the frequency coordinate.

$$I = IDWT\{LL, LH, HL, HH\} \quad (8)$$

### 3.5.2 Extraction

The same flow of DWT and DCT transformations is applied to the watermarked image during extraction. Based on the stored embedding position information and the  $\alpha$  value from the embedding process, two AC coefficients in each block are accessed and normalized by dividing the value of each coefficient by  $\alpha$ . Suppose two selected AC coefficients at positions  $ac1$  and  $ac2$ . The coefficient values are normalized by Eq. (9).

$$ac1n = \frac{D[ac1]}{\alpha}, ac2n = \frac{D[ac2]}{\alpha} \quad (9)$$

After normalization, the relationship between the values of the two coefficients is used to determine the inserted watermark bits using Eq. (10).

$$\begin{cases} \text{if } ac1n < ac2n, \hat{w} = 1 \\ \text{otherwise, } \hat{w} = 0 \end{cases} \quad (10)$$

The extracted bits are then reassembled to form a binary watermark image. The use of  $\alpha$  in the extraction process ensures that the embedded watermark can be accurately retrieved according to the scale applied during Embedding.

## 4. Results and analysis

### 4.1 Dataset and system setup

This section presents the images in the experiment, the software and libraries used, and the quantum-based watermark insertion process settings. The image dataset used is taken from the USC-SIPI Image Database [28], where the samples used can be seen in Figure 3. The images are grayscale images with dimensions of  $512 \times 512$  pixels. For "Baboon", "F-16" and "Peppers" are RGB images converted to grayscale images using the `convert('L')` function from the Python Imaging Library (PIL) to ensure uniformity across all images in the watermark

insertion process. While the watermark has a size of  $32 \times 32$  pixels with a binary format.

The watermarking method in this study was implemented using Python, the Penylane quantum simulator, and several important libraries. PennyLane is the simulator for quantum computing in designing and executing QVC quantum circuits. PIL is used for image processing tasks such as loading images, converting RGB images to grayscale, and storing images that have been watermarked. NumPy is used to handle image data as arrays and for numerical operations. The SciPy library provides important functions for applying DCT and IDCT transformations, which are crucial in watermark embedding in the frequency domain. The matplotlib library is used to visualize the experimental results and plot the structure of the quantum circuit.

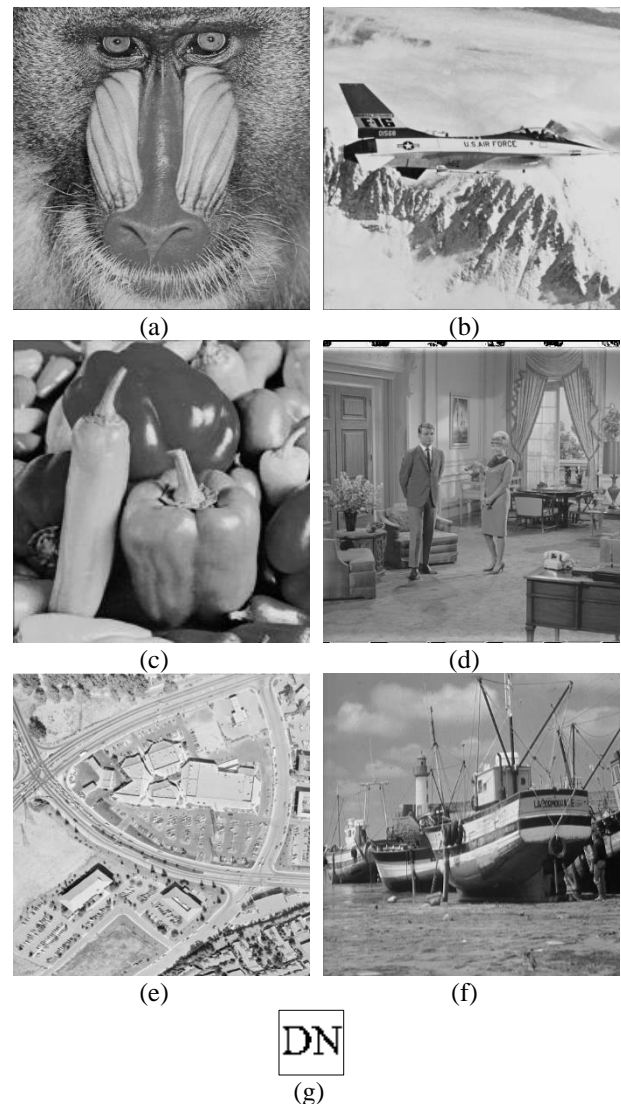


Figure 3 Sample image dataset: (a) 4.2.03 a.k.a Baboon, (b) 4.2.05 a.k.a F-16, (c) 4.2.07 a.k.a Peppers, (d) 5.2.08 a.k.a Couple, (e) 5.2.09 a.k.a Aerial, (f) boat.512, and (g) Binary watermark image

## 4.2 Watermarked quality evaluations

To assess the quality of the watermarked images, we utilized two standard metrics, i.e., Peak Signal-to-Noise Ratio (PSNR) and Structural Similarity Index (SSIM). PSNR measures the ratio between the maximum possible power of a signal and the power of corrupting noise that affects the fidelity of its representation, providing insight into the quality degradation after embedding. A higher PSNR value indicates less distortion in the watermarked image [29]. The PSNR metric is calculated as Eq. (11).

$$PSNR = 10 \cdot \log_{10} \left( \frac{max^2}{\frac{1}{MN} \sum_{i=0}^{M-1} \sum_{j=0}^{N-1} [I(i,j) - I_w(i,j)]^2} \right) \quad (10)$$

Where  $max$  is the maximum pixel value of the image, in this context largest value is 255;  $M$  and  $N$  are image dimensions;  $I$  represent the original image;  $I_w$  represent a watermarked image;  $i, j$  are image pixel coordinates.

Table 1 presents the results of PSNR measurements and comparisons with several related studies. The comparison is valid as PSNR is a standard metric for evaluating image quality, and all methods were tested under comparable conditions using the same datasets[28].

SSIM assesses the perceptual similarity between the original and watermarked images based on changes in luminance, contrast, and structure. In this context, SSIM values range commonly from 0 to 1, where values closer to 1 indicate higher similarity. SSIM is calculated using Eq. (12).

$$SSIM(x, y) = \frac{(2\mu_x\mu_y + C_1)(2\sigma_{xy} + C_2)}{(\mu_x^2 + \mu_y^2 + C_1)(\sigma_x^2 + \sigma_y^2 + C_2)} \quad (12)$$

Table 1. PSNR Results and Comparison

Image	Ref [8]	Ref [11]	Ref [15]	Ref [21]	Ours
Baboon	-	-	-	36.19	45.86
F-16	-	41.15	41.13	36.25	45.58
Peppers	45.66	41.66	40.92	36.18	47.01
Couple	-	-	-	-	46.78
Aerial	-	-	-	-	47.23
Boat	45.09	-	40.05	-	47.70

Table 2. SSIM Results and Comparison

Image	Ref [8]	Ref [15]	Ref [21]	Ours
Baboon	-	-	0.9702	0.9977
F-16	-	0.9992	0.9705	0.9980
Peppers	0.982	0.9990	0.9504	0.9975
Couple	-	-	-	0.9986
Aerial	-	-	-	0.9985
Boat	0.987	0.9996	-	0.9976

Where  $\mu_x$  and  $\mu_y$  are the means,  $\sigma_x^2$  and  $\sigma_y^2$  are variances,  $\sigma_{xy}$  is the covariance, and  $C_1$  and  $C_2$  are constants.

In the same way as PSNR measurements, we also performed SSIM measurements and comparisons with several related studies, presented in Table 2.

Evaluation of the quality of watermarked images using PSNR and SSIM metrics. As presented in Table 1, the average PSNR value for all test images is 46.93 dB, indicating that the watermarked images have high similarity to the original cover images. The SSIM results, as presented in Table 2, show an average similarity score of 0.9979, highlighting that the embedding process results in minimal visual degradation.

Compared with existing methods, this approach performs better in maintaining image quality. For example, the method in [8] achieves a PSNR of 45.66 dB for the Peppers image. In addition, based on the PSNR, our results appear to be dominantly better on all images. Unfortunately, based on the SSIM value, the proposed method is indeed not better than the method [15], but the results are very competitive with a minimal difference in SSIM values, and still better than the study [8], with our method, which shows a better level of imperceptibility when looking at both measuring instruments.

## 4.3 Robustness under various attack evaluations

Various attacks, such as JPEG compression, cropping, and noise addition, are tested at this stage. In the robustness evaluation, Normalized Correlation (NC) is used. NC is a standard metric used in watermarking evaluation, which measures the similarity between the extracted watermark and the original watermark after the image is attacked. NC values close to 1 indicate that the watermark is well preserved, while lower values indicate degradation or loss of the watermark. NC can be calculated by Eq. (13).

$$NC = \frac{\sum_{i=1}^M \sum_{j=1}^N W(i,j) \cdot W'(i,j)}{\sqrt{\sum_{i=1}^M \sum_{j=1}^N W(i,j)^2} \sqrt{\sum_{i=1}^M \sum_{j=1}^N W'(i,j)^2}} \quad (13)$$

Where  $W(i,j)$  is the original watermark pixel value at position  $i,j$ ;  $W'(i,j)$  is the extracted watermark pixel value at position  $i,j$ .

The NC has been widely used as a robustness measurement tool. So, in this section, measurements are also carried out with NC, which are presented in Table 3. In addition, a fair comparison is also carried out with the same type of attack, attack parameters, and image (pepper image) presented in Table 4.

The robustness of the proposed method is evaluated using the NC metric, as shown in Table 3. The average NC value for all attack scenarios is 0.9752, indicating the robustness of the watermark against various distortions, including JPEG compression, noise addition, resizing, and cropping. Table 4 highlights the robustness of our method on Peppers images compared to [8] and [15]. Specifically, in the JPEG compression scenario with Q=20, our method achieves an NC of 0.8463, which is competitive compared to [8], where the NC value drops to 0.7497. In addition, for the median filter (3×3 kernel) and resizing attacks, our approach consistently maintains an NC value close to 1.0, indicating a near-perfect success rate of watermark extraction under these conditions. In the Gaussian noise scenario with a variance of 0.001, our NC value is 0.9598, which is superior to [8], which achieves 0.9702. Overall, the proposed method is mostly superior to previous studies. These results demonstrate the effectiveness of quantum-based optimization in improving robustness without sacrificing the visual quality of the watermark.

Table 3. Average NC measurement results from all images

Attack types	Parameter	NC
Free	-	1.0
JPEG compression	Q=70	0.9998
JPEG compression	Q=40	0.9857
JPEG compression	Q=20	0.8463
Median Filter (MF)	3×3	0.9998
Salt and pepper noise (SPN)	0.01	0.9969
Gaussian noise (GN)	0.001	0.9598
Resizing	512-256-512	0.9998
Cropping	100×100 center	0.9887

Table 4. NC comparison results for peppers Image

Attack types	Ref [8]	Ref [15]	Ours
Free	1.0	1.0	1.0
JPEG Q=70	-	0.7927	1.0
JPEG Q=40	1.0	-	0.9879
JPEG Q=20	0.7497	-	0.8324
MF 3×3	1.0	0.9596	1.0
SPN	-	0.9312	0.9970
GN	0.9702	-	0.9590
Resizing	1.0	-	1.0
Cropping	0.9610	0.9972	0.9893

## 5. Conclusion

This study has successfully developed a DWT-DCT-based watermarking method with quantum optimization, which integrates Quantum-Inspired Annealing (QIA) to determine the optimal AC coefficient position in the DCT domain and Quantum Variational Circuits (QVC) to adjust the embedding intensity adaptively. The evaluation shows that the proposed method performs better in preserving visual quality with an average PSNR of 46.93 dB and SSIM of 0.9979, indicating minimal distortion in the image after the embedding process. In the resistance test against various attacks, this method shows significant strength with an average NC value of 0.9752, indicating that the watermark can still be extracted with high accuracy. Compared with previous studies, the proposed method performs better in most metrics, especially in the JPEG compression and Gaussian noise attack scenarios.

This approach's main advantage lies in combining quantum-based optimization with domain transformation, which allows for increased watermark robustness without sacrificing image quality. This study opens up opportunities for further exploration in the development of quantum computing-based watermarking, especially for applications in data environments with high levels of manipulation. In the future, additional testing in a broader dataset and variations of quantum parameters can be performed to improve the generalization and scalability of the proposed method.

## Conflicts of Interest

The authors declare no conflict of interest.

## Author Contributions

Conceptualization, NR and DRIMS; methodology, NR and DRIMS; software, DRIM; validation, SKG, AKS, and AS; formal analysis, SKG, AKS, and AS; investigation, NR and DRIMS;

resources, NR; data curation, DRIMS; writing—original draft preparation, NR and DRIMS; writing—review and editing, all; visualization, DRIMS; supervision, DRIMS; project administration, NR; funding acquisition, NR.

## References

- [1] A. Setyono and D. R. I. M. Setiadi, “An Image Watermarking Method Using Discrete Tchebichef Transform and Singular Value Decomposition Based on Chaos Embedding”, *Int. J. Intell. Eng. Syst.*, Vol. 13, No. 2, pp. 140–150, 2020, doi: 10.22266/ijies2020.0430.14.
- [2] N. Rijati, P. N. Andono, and D. R. I. M. Setiadi, “Imperceptible Improvement using Edge Area Selection for Robust Video Watermarking Using Tchebichef - Singular Value Decomposition”, *Int. J. Intell. Eng. Syst.*, Vol. 15, No. 2, pp. 298–306, 2022, doi: 10.22266/ijies2022.0430.27.
- [3] I. Assini, A. Badri, K. Safi, A. Sahel, and A. Baghdad, “A Robust Hybrid Watermarking Technique for Securing Medical Image”, *Int. J. Intell. Eng. Syst.*, Vol. 11, No. 3, 2018, doi: 10.22266/ijies2018.0630.18.
- [4] Y. S. Lee, Y. H. Seo, and D. W. Kim, “Digital blind watermarking based on depth variation prediction map and DWT for DIBR free-viewpoint image”, *Signal Process. Image Commun.*, Vol. 70, No. September 2018, pp. 104–113, 2019, doi: 10.1016/j.image.2018.09.004.
- [5] U. Sudibyo, F. Eranisa, E. H. Rachmawanto, D. R. I. M. Setiadi, and C. A. Sari, “A secure image watermarking using Chinese remainder theorem based on haar wavelet transform”, In: *Proc. of 2017 4th International Conference on Information Technology, Computer, and Electrical Engineering*, 2018, doi: 10.1109/ICITACEE.2017.8257704.
- [6] H. Wang, Z. Yuan, S. Chen, and Q. Su, “Embedding color watermark image to color host image based on 2D-DCT”, *Optik (Stuttg)*, Vol. 274, No. January, p. 170585, 2023, doi: 10.1016/j.ijleo.2023.170585.
- [7] M. Moosazadeh and G. Ekbatanifard, “A new DCT-based robust image watermarking method using teaching-learning-Based optimization”, *J. Inf. Secur. Appl.*, Vol. 47, pp. 28–38, 2019, doi: 10.1016/j.jisa.2019.04.001.
- [8] V. Sisaudia and V. P. Vishwakarma, “A secure gray-scale image watermarking technique in fractional DCT domain using zig-zag scrambling”, *J. Inf. Secur. Appl.*, Vol. 69, No. July, p. 103296, 2022, doi: 10.1016/j.jisa.2022.103296.
- [9] J. Sang, Q. Liu, and C.-L. Song, “Robust video watermarking using a hybrid DCT-DWT approach”, *J. Electron. Sci. Technol.*, Vol. 18, No. 2, p. 100052, 2020, doi: 10.1016/j.jnlest.2020.100052.
- [10] C. A. Sari, E. H. Rachmawanto, and D. R. I. M. Setiadi, “Robust and imperceptible image watermarking by DC coefficients using singular value decomposition”, In: *Proc. of International Conference on Electrical Engineering, Computer Science and Informatics (EECSI)*, 2017, doi: 10.1109/EECSI.2017.8239107.
- [11] H. J. Ko, C. T. Huang, G. Horng, and S. J. WANG, “Robust and blind image watermarking in DCT domain using inter-block coefficient correlation”, *Inf. Sci. (Ny)*, vol. 517, pp. 128–147, 2020, doi: 10.1016/j.ins.2019.11.005.
- [12] G. Budiman, L. Novamizanti, and I. Iwut, “Genetics algorithm optimization of DWT-DCT based image Watermarking”, *J. Phys. Conf. Ser.*, Vol. 795, No. 1, p. 012039, 2017, doi: 10.1088/1742-6596/795/1/012039.
- [13] S. Hossain, S. Mukhopadhyay, B. Ray, S. K. Ghosal, and R. Sarkar, “A secured image steganography method based on ballot transform and genetic algorithm”, *Multimed. Tools Appl.*, Vol. 81, No. 27, pp. 38429–38458, 2022, doi: 10.1007/s11042-022-13158-7.
- [14] H. Gao and Q. Chen, “A robust and secure image watermarking scheme using SURF and improved Artificial Bee Colony algorithm in DWT domain”, *Optik (Stuttg)*, Vol. 242, No. March, p. 166954, 2021, doi: 10.1016/j.ijleo.2021.166954.
- [15] A. Melman and O. Evsutin, “Image watermarking based on a ratio of DCT coefficient sums using a gradient-based optimizer”, *Comput. Electr. Eng.*, Vol. 117, No. March, p. 109271, 2024, doi: 10.1016/j.compeleceng.2024.109271.
- [16] H. T. Hu, L. Y. Hsu, and T. T. Lee, “All-round improvement in DCT-based blind image watermarking with visual enhancement via denoising autoencoder”, *Comput. Electr. Eng.*, Vol. 100, No. February, p. 107845, 2022, doi: 10.1016/j.compeleceng.2022.107845.
- [17] C. C. McGeoch, “Quantum Annealing”, *Adiabatic Quantum Computation and Quantum Annealing*, pp. 29–42, 2014, doi: 10.1007/978-3-031-02518-1\_3.

- [18] S. Dhar and A. K. Sahu, “Digital to quantum watermarking: A journey from past to present and into the future”, *Comput. Sci. Rev.*, Vol. 54, No. June, p. 100679, 2024, doi: 10.1016/j.cosrev.2024.100679.
- [19] M. Cerezo *et al.*, “Variational quantum algorithms”, *Nat. Rev. Phys.*, Vol. 3, No. 9, pp. 625–644, 2021, doi: 10.1038/s42254-021-00348-9.
- [20] R. Y. Abadi and P. Moallem, “Robust and optimum color image watermarking method based on a combination of DWT and DCT”, *Optik (Stuttg)*, Vol. 261, No. December 2021, p. 169146, 2022, doi: 10.1016/j.ijleo.2022.169146.
- [21] Z. Xing, C.-T. Lam, X. Yuan, G. Huang, and P. Machado, “A novel geometrically invariant quantum watermarking scheme utilizing Quantum Error Correction”, *J. King Saud Univ. - Comput. Inf. Sci.*, Vol. 35, No. 10, p. 101818, 2023, doi: 10.1016/j.jksuci.2023.101818.
- [22] Z. Xing, X. Yuan, and C.-T. Lam, “A Quantum Watermarking Scheme Using New Enhanced Quantum Image Representation”, In: *Proc. of 2023 8th International Conference on Signal and Image Processing (ICSIP)*, pp. 326–330, 2023, doi: 10.1109/ICSIP57908.2023.10270930.
- [23] R. F. Aly, “New quantum color image watermarking technique (NQCIWT)”, *Soft Comput.*, Vol. 28, No. 17–18, pp. 10177–10186, 2024, doi: 10.1007/s00500-024-09739-3.
- [24] A. Winarno, D. R. I. M. Setiadi, A. A. Arrasyid, C. A. Sari, and E. H. Rachmawanto, “Image watermarking using low wavelet subband based on 8×8 sub-block DCT”, In: *Proc. of 2017 International Seminar on Application for Technology of Information and Communication (iSemantic)*, pp. 11–15, 2017, doi: 10.1109/ISEMANTIC.2017.8251835.
- [25] O. Lockwood, “An Empirical Review of Optimization Techniques for Quantum Variational Circuits”, *arXiv*. 2022, [Online]. Available: <https://arxiv.org/abs/2202.01389>
- [26] C. Bernhardt, *Quantum Computing for Everyone*. Fairfield University: The MIT Press, 2019. doi: 10.7551/mitpress/11860.001.0001.
- [27] A. N. Safriandono, D. R. I. M. Setiadi, A. Dahlan, F. Z. Rahmanti, I. S. Wibisono, and A. A. Ojugo, “Analyzing Quantum Feature Engineering and Balancing Strategies Effect on Liver Disease Classification”, *J. Futur. Artif. Intell. Technol.*, Vol. 1, No. 1, pp. 51–63, 2024, doi: 10.62411/faith.2024-12.
- [28] USC Viterbi School of Engineering, “SIPI Image Database”, <http://sipi.usc.edu/database/> (accessed Mar. 27, 2019).
- [29] C. Rupa, R. P. Malleswari, S. A. Sultana, M. Abbas, and A. K. Sahu, “Data Privacy Protection Using Lucas Series Based Hybrid Reversible Watermarking Approach”, *IEEE Access*, Vol. 12, pp. 134578–134593, 2024, doi: 10.1109/ACCESS.2024.3459041.

## Appendix

Table 5. Notation List

Notation	Definition
$I$	Cover Image
$I_w$	Watermarked Image
$W$	Watermark Image
$W'$	Extracted Watermark Image
$\hat{w}$	Extracted Watermark bit value
$M, N$	Image dimension
$i, j$	image pixel coordinates in spatial state
$\alpha$	Embedding intensity parameter.
$DWT$	Discrete Wavelet Transform
$LL, LH, HL, HH$	Subbands from DWT decomposition.
$DCT$	Discrete Cosine Transform
$B$	Subblock 8×8 (spatial)
$D$	Subblock 8×8 (transformed)
$AC$	Alternating Current coefficients in the DCT domain
$DC$	Direct Current coefficient in the DCT domain
$u, v$	image pixel coordinates in transformation state (DCT)
$NC$	Normalized Correlation, measuring robustness of extracted watermark.
$H$	Hadamard gate for quantum superposition.
$\theta$	Rotation angle for quantum gates
$RZ, RX, RY$	Quantum rotation gates around the z, x, and y-axis, respectively
$CNOT$	Controlled-NOT gate for entanglement in quantum computing
$\alpha$	Embedding intensity parameter
$QIA$	Quantum-Inspired Annealing for optimizing embedding positions.
$QVC$	Quantum Variational Circuit for adaptive embedding intensity.
$q_i$ or $q_j$	$i^{\text{th}}$ or $j^{\text{th}}$ qubit
$n$	Number of qubits or data points used in the quantum circuit or summation
$\langle Z_i \rangle$	Expectation value of the Pauli-Z operator for qubit $i$ .

$L(P, \alpha)$	Loss function used for optimizing embedding parameters, where $P$ is the embedding position.
$ \psi(\theta)\rangle$	the final result of a variational quantum circuit